Synthesis, thermogravimetric and high temperature X-ray diffraction analyses of zinc-substituted nickel manganites

C. Chanel[a], S. Fritsch[a,*], C. Drouet[a], A. Rousset[a], M.L. Martínez Sarrión[b], L. Mestres[b], M. Morales[b]

[a]*Laboratoire de Chimie des Matériaux Inorganiques, ESA 5070, Université Paul Sabatier, 118, Route de Narbonne, 31062 Toulouse Cedex, France*
[b]*Departament de Química Inorgànica, Universitat de Barcelona, Diagonal 647, 08028 Barcelona, Spain*

Abstract

Stoichiometric spinel phases $Mn_{2.35-x}Ni_{0.65}Zn_xO_4$ were prepared by thermal decomposition of mixed oxalate precursor powders $Mn_{0.78-\alpha}Ni_{0.22}Zn_\alpha C_2O_4 \cdot nH_2O$ (with $0 \leq \alpha \leq 0.53$) at 900°C. Cation-deficient phases $Mn_{2.35-x}Ni_{0.65}Zn_x\square_{3\delta/4}O_{4+\delta}$ were identified in the temperature range 350–500°C. The nonstoichiometric coefficient δ was found to strongly depend on the zinc content and the decomposition temperature. We showed that the introduction of zinc into the spinel phase enlarges the stability domain of the structure and inhibits oxidation at least up to 900°C. A cubic single-phase was observed for $x \leq 1.00$. The lattice parameter variation of the oxides in the composition range $0 \leq x \leq 0.60$ can be explained using Poix's method, in terms of the distribution of Zn^{2+} cations on the tetrahedral sites. However, for higher zinc content ($x > 0.6$) a detailed analysis of data showed that a small fraction of Zn^{2+} is located on octahedral sites.

Keywords: A. Oxides; B. Chemical synthesis; C. X-ray diffraction; C. Thermogravimetric analysis (TGA)

* Corresponding author. Fax: +33-5-61-61-63.
E-mail address: fritsch@ramses.ups-tlse.fr (S. Guillemet-Fritsch).

1. Introduction

The Mn/Ni/O system with spinel structure has been widely studied [1–8], especially in view of its commercial application as negative temperature thermistor ceramics. These spinel phases are usually obtained at temperatures above 850–900°C by thermal decomposition in air of mixed oxalate salt precursors. Recent studies [9–12] have shown that these spinel phases can be obtained at low temperatures (300–400°C); however, they present cation deficiencies due to oxygen excess. Moreover, these phases decompose with increasing temperatures, giving rise to thermodynamically stable phases $NiMnO_3$ and α-Mn_2O_3 in the temperature range 500–800°C. At 900°C, a stoichiometric spinel phase is obtained. On the other hand, it has been shown [13,14] that zinc substitution in hausmannite leads to a stabilization of the spinel phase, i.e., to an inhibition of oxidation phenomena.

The aim of this work was to synthesize and characterize a mixed zinc-nickel-manganese oxalate series $Mn_{0.78-\alpha}Ni_{0.22}Zn_\alpha C_2O_4{\cdot}nH_2O$ ($0 \leq \alpha \leq 0.53$).

2. Experimental

2.1. Elaboration of the oxalate precursors

Samples of the series $Mn_{0.78-\alpha}Ni_{0.22}Zn_\alpha C_2O_4{\cdot}nH_2O$ ($0 \leq \alpha \leq 0.53$) were prepared by coprecipitation of transition metal nitrates $Mn(NO_3)_2{\cdot}6H_2O$, $Ni(NO_3)_2{\cdot}6H_2O$, and $Zn(NO_3)_2{\cdot}6H_2O$ with ammonium oxalate $(NH_4)_2C_2O_4{\cdot}H_2O$ in an aqueous solution at 25°C. The precipitates were stirred for 30 min, then filtered, washed several times with deionized water, and dried in air at 60°C. The precipitation reaction is described in Eq. (1):

$$\begin{aligned}&(0.78 - \alpha)\,Mn(NO_3)_2{\cdot}6H_2O + 0.22Ni(NO_3)_2{\cdot}6H_2O + \\ &\quad \alpha\text{-}Zn(NO_3)_2{\cdot}6H_2O + (NH_4)_2C_2O_4{\cdot}H_2O \downarrow \\ &Mn_{0.78-\alpha}Ni_{0.22}Zn_\alpha C_2O_4{\cdot}nH_2O + 2NO_3^- + 2NH_4^+ + (7 - n)\,H_2O \end{aligned} \quad (1)$$

2.2. Characterization techniques

The powder morphology was observed with a JEOL JSM-6400 scanning electron microscope. The thermal decomposition of the mixed oxalate precursors was examined by thermogravimetric analysis (Setaram TGDTA92B operating in air) and high temperature X-ray diffraction analysis (Bragg-Brentano $\theta/2\theta$ Siemens D500 powder diffractometer, using Cu Kα radiation ($\lambda_1 = 1.54060$ Å, $\lambda_2 = 1.54443$ Å, $\lambda_2/\lambda_1 = 0.50$) and operating at 40 kV and 30 mA). Data were collected in the step-scan mode using 0.02° 2θ step-size and 1s/step counting time over the 2θ range 20–80°. The chemical composition of the oxides was determined by plasma emission spectrometry.

Temperature programmed reduction analyses (TPR) were performed both by thermogravimetry and gas chromatography. Experiments were realized in a vertical plug flow differential reactor. The mass variation was determined with a Cahn D200 microbalance

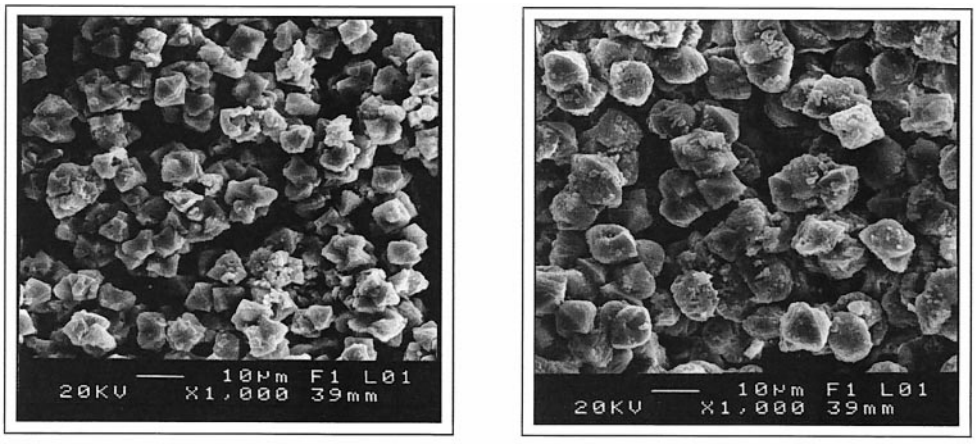

a) $\alpha = 0.00$ b) $\alpha = 0.39$

Fig. 1. SEM micrographs of zinc nickel manganese oxalate $Mn_{0.78-\alpha}Ni_{0.22}Zn_{\alpha}C_2O_4 \cdot nH_2O$: (a) $\alpha = 0.00$, (b) $\alpha = 0.39$.

(accuracy 10^{-6}g). The temperature of the sample could be linearly increased by a furnace monitored by a Shimaden SR25 temperature programmer. The sample was first degassed (1 Pa) at room temperature for 1 h, then the system was filled with Ar. A flow of 15 cm^3min^{-1} was allowed to pass through the reactor. During the experiment, the temperature was linearly increased to 950°C (with a heating rate $\beta = 5°Cmin^{-1}$). Every 120 s, the gas flowing out of the reactor was sampled and analyzed by gas chromatography (Shimadzu GC-8A chromatograph fitted with a molecular sieve 13× column and a thermal conductivity detector). These analyses measured the oxygen concentration in the flowing gas, and the integration of these data over time gave the total amount of oxygen released during the experiment.

3. Results and discussion

3.1. Characterization of the zinc-nickel-manganese oxalates

The powder morphology was shown to depend on the zinc content. For low zinc content, the powder has an octahedral-like shape. It becomes more spherical as the zinc content increases (Fig. 1). The average size of the oxalate powders varies between 10 and 15 μm.

It is well established [15] that nickel manganese oxalate $Mn_{1-\alpha}Ni_{\alpha}C_2O_4 \cdot 2H_2O$ synthesized by "chimie douce" is a mixed oxalate that crystallizes in the stable α form, for nickel content $\alpha \leq 0.25$. X-ray diffraction experiments completed with TG analyses show that the substitution of Mn by Zn in this system leads to mixed oxalates. High temperature X-ray diffraction was performed to follow the oxalate structural change (Table 1).

In the nickel manganese oxalate TG curve (Fig. 2), a continuous weight loss between 350 and 500°C (Step I) was observed. This mass loss was also observed for oxides containing zinc, although it decreased with increasing zinc content. In this temperature range, it was difficult to

Table 1
Structural evolution of mixed $Mn_{0.78-\alpha}Ni_{0.22}Zn_{\alpha}C_2O_4{\cdot}2H_2O$ oxalates as a function of temperature for different zinc contents α

T (°C)	α					
	0.00	0.10	0.21	0.34	0.39	0.45
300, 1 h	AP	AP	AP	Csp_{PCP}	AP	AP
400, 1 h	AP	AP	Csp_{PCP}	Csp_{PCP}	AP	AP
500, 1 h	$NiMnO_3$ + α-Mn_2O_3	Csp_{PCP}	Csp_{PCP}	Csp	Csp_{PCP}	Csp_{PCP} + ZnO_{PCP}
600, 1 h	$NiMnO_3$ + α-Mn_2O_3	$NiMnO_3$ + α-Mn_2O_3 + Csp_{PCP}	Csp	Csp	Csp	Csp_{PCP} + ZnO_{PCP}
700, 1 h	$NiMnO_3$ + α-Mn_2O_3	α-Mn_2O_3 + $NiMnO_3$ + Csp_{PCP}	Csp	Csp	Csp	Csp + ZnO
800, 1 h	Csp + $NiMnO_3$ + α-Mn_2O_3	Csp + α-Mn_2O_3 + $NiMnO_3$[a]	Csp	Csp	Csp	Csp + ZnO
900, 4 h	Csp	Csp	Csp	Csp	Csp + Zno[a]	Csp + ZnO

Csp: Cubic spinel; AP: Amorphous phases; PCP: Poorly crystallized phases.
[a]Small amount.

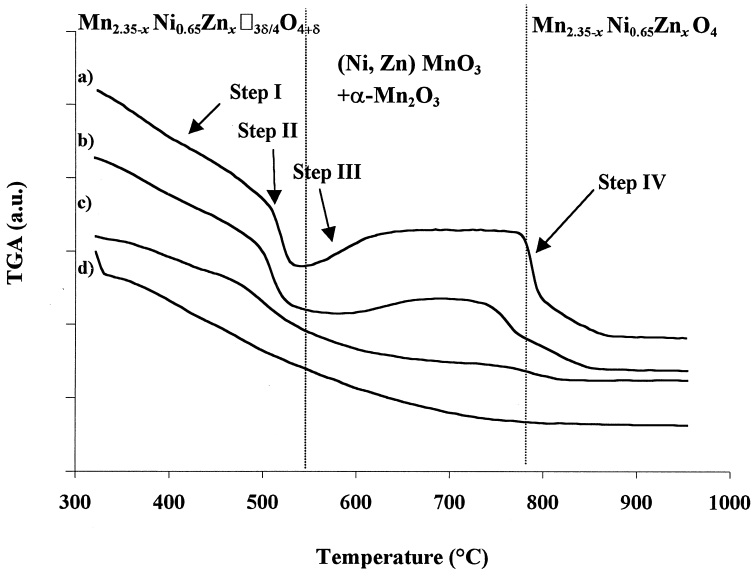

Fig. 2. TG curves of $Mn_{2.35-x}Ni_{0.65}Zn_xO_4$, with (a) x = 0.00, (b) x = 0.11, (c) x = 0.31, and (d) x = 0.62, in the temperature range 300–1000°C.

identify the structure using in situ XRD analysis because the phase was almost amorphous. However, previous studies [9–12,16] have shown that a nonstoichiometric spinel phase $Mn_{2.35}Ni_{0.65}\square_{3\delta/4}O_{4+\delta}$ (with oxygen excess) is obtained. We find that in a similar temperature range, the spinel phase is more crystallized (and therefore identified) and appears at lower temperature as the zinc content increases. The nonstoichiometry coefficient δ was determined by TPR experiments for the low temperature (400°C) $Mn_{2.35-x}Ni_{0.65}Zn_x\square_{3\delta/4}O_{4+\delta}$ phases as a function of zinc content (Table 2). δ decreased significantly with increasing zinc content. On the other hand, for a fixed zinc content (x = 0.00 and x = 0.31) (Table 3), the nonstoichiometric coefficient δ decreased with increasing decomposition temperature.

From these results, one can assume that the weight loss observed on the TG curve between 350 and 500°C corresponds to the oxygen excess of the nonstoichiometric phases. In fact, when the zinc content increases, the mass loss observed is less important, which is in agreement with the variations of δ. At 520°C (Step II), the sudden mass loss observed for nickel manganese oxalate (Fig. 2, curve a) is due to the reduction of the octahedral Mn^{4+} cations to Mn^{3+} or Mn^{2+}. According to Tang et al. [10], the reduction could be related to the migration of Ni^{2+} and Mn^{2+} from the octahedral to the tetrahedral sites. In the temperature range 550–900°C, the mass changes observed (Steps III and IV) are due to the oxidation of the tetrahedral Mn^{2+} cations to Mn^{3+}, which leads to the

Table 2
Nonstoichiometric coefficient δ at 400°C as a function of zinc content x

x	0.00	0.31	0.70	1.02
$\delta_{400°C}$	0.51	0.32	0.24	0.16

Table 3
Nonstoichiometric coefficient δ as a function of decomposition temperature

	x = 0.00	x = 0.31
$\delta_{350°C}$	0.66	0.30
$\delta_{400°C}$	0.51	0.30
$\delta_{420°C}$	0.24	0.26

transformation of the spinel phase into the bixbyite α-Mn_2O_3 (JCPDS file 24-0508) and the ilmenite $NiMnO_3$ (JCPDS file 12-0269) [6,16–18]. The mass loss (Step IV) is due to the reaction of these two phases to form the cubic spinel phase again. After 4 h at 900°C, only the spinel phase $Mn_{2.35}Ni_{0.65}O_4$ is observed, as expected. The mass change related to this reduction decreases rapidly as the zinc content increases, and disappears for $\alpha > 0.10$. For this composition, the diffraction peaks relative to the $NiMnO_3$ and α-Mn_2O_3 phases are no longer observed. In fact, the temperature range of stability increases significantly with increasing zinc content. However, if the zinc content is too high ($\alpha > 0.34$), the ZnO phase is observed (JCPDS file 36-1451) in addition to the cubic spinel phase (Table 1). As expected, the precipitation of ZnO occurs at lower temperatures as the ratio of zinc increases. So the substitution of manganese by zinc in solid solution series $Mn_{2.35-x}Ni_{0.65}Zn_xO_4$ results in a gradual and substantial change in the thermal behavior of the oxides in the temperature range 300–900°C. We can say that the introduction of zinc into the spinel phase enlarges the stability domain of the structure and inhibits oxidation at least up to 900°C. Our results are in agreement with those obtained by Dubrawski [14]. He showed the increase of stability of hausmannite Mn_3O_4 when introducing zinc in the structure. Fruhwirth et al. [19] mentioned the role of zinc cations in the increasing stability of the structure in Mn/Ni/Zn/O systems.

3.2. Characterization of the zinc-nickel-manganese oxides

For this part of the work, the temperature of the treatment was fixed at 900°C for 4 h in air. At this temperature, a single phase is obtained for the composition range from $Mn_{2.33}Ni_{0.67}O_4$ to $Mn_{1.33}Ni_{0.65}Zn_{1.02}O_4$ (Fig. 3). The heating and cooling rates were fixed at 150°C/h. One single spinel phase is observed up to $x \leq 1.1$. For higher zinc content, the ZnO phase appears. The experimental lattice parameter a_{exp} decreases linearly as the zinc content increases, in agreement with Vegard's law. It is well established that Zn^{2+} cations are located on the tetrahedral sites in zinc manganites [20,21]. The strong tetrahedral preference of Zn^{2+} cation was evidenced by electrostatic energy measurements by O'Neill and Navrotsky [22]. In fact, the ionic radius of Zn^{2+} is smaller than that of Mn^{2+} ($r_{Zn^{2+}} = 0.580$ Å and $r_{Mn^{2+}} = 0.655$ Å) in the tetrahedral sites [22]. The decrease of the lattice parameters is similar to that observed by Feltz and Seidel [23] in the $Mn_{2-x}Ni_{1.00}Zn_xO_4$ system. When the ZnO phase appears, the lattice parameter of the spinel phase is constant.

The spinel structure is based on the cubic close-packing of oxygen ions in which the cations are located on both tetrahedral and octahedral sites. The general formula for the cationic distribution is

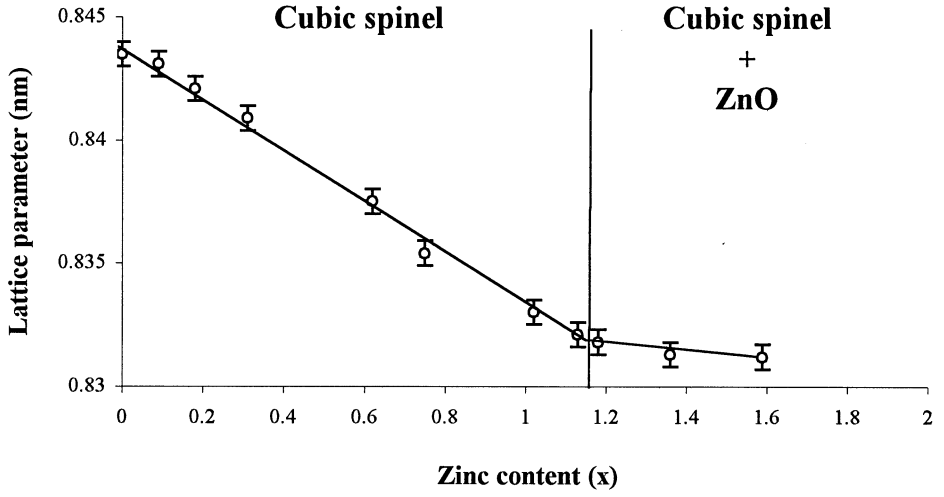

Fig. 3. Variation of the experimental lattice parameter of the spinel phase in $Mn_{2.35-x}Ni_{0.65}Zn_xO_4$ oxide as a function of zinc content (x).

$$A^{2+}_{1-2\lambda}B^{3+}_{2\lambda}[B^{3+}_{2-2\lambda}A^{2+}_{2\lambda}]O^{2-}_4 \quad (2)$$

where λ is the degree of inversion, $0 \leq \lambda \leq 0.5$. The brackets indicate the octahedral sites.

Poix [24] has pointed out the invariable character of the "anion–cation" distance for a particular site in the spinel structure. Thus two parameters are defined, d_{CA} = A–O and d_{CB} = B–O, where d_{CA} and d_{CB} are the mean values of the "anion–cation" distance in tetrahedral and octahedral sites, respectively. The lattice parameter a is related to d_{CA} and d_{CB} according to the following relation:

$$a = 2.0995d_{CA} + \sqrt{(5.8182d^2_{CB} - 1.4107d^2_{CA})} \quad (3)$$

The theoretical lattice parameters can be calculated for various cationic distributions and compared with the experimental parameters. Therefore, the cationic distribution of a solid solution can be approached. We want to point out that this method is qualitative, and we will consider only the single phases for determining a cationic distribution. The characteristic bond lengths Mn–O, Ni–O, Zn–O on the different sites are found in ref. 24. The zinc nickel manganites were prepared by substituting manganese cations by zinc in nickel manganites of formula $Mn_{2.35}Ni_{0.65}O_4$. Under the same preparation conditions, Legros et al. [25] proposed a cationic distribution for nickel manganites $Mn_{3-x}Ni_xO_4$ ($0.5 \leq x \leq 1$):

$$Mn^{2+}_{1-y}Ni^{2+}_y[Ni^{2+}_{x-y}Mn^{3+}_{2-2(x-y)}Mn^{4+}_{x-y}]O^{2-}_4 \quad (4)$$

where $y = xP/100$ and P = percentage of Ni^{2+} on tetrahedral sites; $P = f(x) = -82.1x^2 + 192.4x - 81.5$.

In fact, despite their strong preference for octahedral sites, a small fraction of Ni^{2+} cations is located on the tetrahedral sites. In order to keep the electroneutrality, the number of Mn^{4+} cations on octahedral sites is equal to that of Ni^{2+} cations on the same sites. Gillot et al. [26] have quantified the degree of inversion, using neutron diffraction experiments, for a given

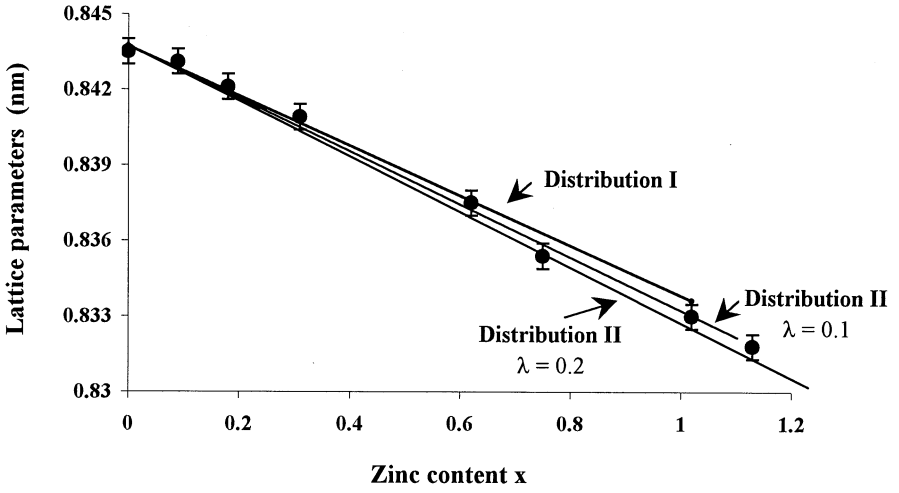

Fig. 4. Variation of the lattice parameter calculated (using Poix's method) for cationic distributions I, II, and experimental, as a function of zinc content. Distribution I: $Mn^{2+}_{1-x}Zn^{2+}_{x}[Ni^{2+}_{0.65}Mn^{3+}_{0.7}Mn^{4+}_{0.65}]O^{2-}_{4}$ ($x \leq 0.6$); Distribution II: $Mn^{2+}_{1-(1-\lambda)x}Zn^{2+}_{(1-\lambda)x}[Ni^{2+}_{0.65}Zn^{2+}_{\lambda}Mn^{3+}_{0.7-2\lambda}Mn^{4+}_{0.65+\lambda}]O^{2-}_{4}$ ($x > 0.6$).

nickel manganite. For the composition $Ni_{1.00}Mn_{2.00}O_4$, only 0.12 Ni^{2+} (per unit formula) is located on the tetrahedral sites. For $Mn_{2.35}Ni_{0.65}O_4$, all the Ni^{2+} are located on the octahedral sites. The variation of the lattice parameter of $Mn_{2.35-x}Ni_{0.65}Zn_xO_4$ as a function of the zinc content x ($0 \leq x \leq 0.35$), calculated for the cationic distribution I, where Zn^{2+} cations are located in tetrahedral sites, is compared with the experimental data in Fig. 4. In all cases, all the Ni^{2+} cations (0.66 per unit formula) are located on the octahedral sites. The limiting cationic distribution (distribution I) proposed is

$$Mn^{2+}_{1-x}Zn^{2+}_{x}[Ni^{2+}_{0.65}Mn^{3+}_{0.7}Mn^{4+}_{0.65}]O^{2-}_{4}(x \leq 0.6) \tag{5}$$

This observation confirms that the Zn^{2+} cations are located on the tetrahedral sites. Thus, in these compounds $Mn_{2.35-x}Ni_{0.65}Zn_xO_4$, the tetrahedral sites are occupied by the zinc ions and the octahedral sites are shared by the nickel and manganese ions. However, for higher zinc content ($x > 0.6$), a small shift is observed between the experimental and the calculated lattice parameter (Fig. 4). In this case, if we consider that a small amount of Zn^{2+} can occupy the octahedral sites, according to distribution II

$$Mn^{2+}_{1-(1-\lambda)x}Zn^{2+}_{(1-\lambda)x}[Ni^{2+}_{0.65}Zn^{2+}_{\lambda}Mn^{3+}_{0.7-2\lambda}Mn^{4+}_{0.65+\lambda}]O^{2-}_{4}(x > 0.6) \tag{6}$$

a much better agreement is obtained. The calculated lattice parameters for, respectively, 10% and 20% of Zn^{2+} located on octahedral sites are plotted in Fig. 4. Although the Zn^{2+} cations preferentially occupy the tetrahedral sites, when the zinc content increases, a small fraction of Zn^{2+} cations could move to the octahedral sites. Two cationic distributions are suggested for different zinc content:

$$\text{For } x \leq 0.6\text{: } Mn^{2+}_{1-x}Zn^{2+}_{x}[Ni^{2+}_{0.65}Mn^{3+}_{0.7}Mn^{4+}_{0.65}]O^{2-}_{4} \tag{7}$$

$$\text{For } x > 0.6\text{: } Mn^{2+}_{1-(1-\lambda)x}Zn^{2+}_{(1-\lambda)x}[Ni^{2+}_{0.65}Zn^{2+}_{\lambda}Mn^{3+}_{0.7-2\lambda}Mn^{4+}_{0.65+\lambda}]O^{2-}_{4} \quad (8)$$

The results are in agreement with the studies of zinc manganites $Mn_{2-x}Zn_{x+1}O_4$ conducted by Rosenberg et al. [27]. They supposed that a fraction of the Zn^{2+} cations was located on the octahedral sites.

Acknowledgments

The authors are grateful to Mrs. R. Legros for her valuable advice and continuous interest in this work. They also thank Mr. P. Alphonse for his assistance in the measurement and interpretation of the TPR analyses, Mr. J. Sarrias for helpful discussion, and Mr. X. Alcobe and Mr. J. Bassas (Servicio de difraccion de rayos X de la Universidad de Barcelona) for their help to obtain high-temperature X-ray diffraction results.

References

[1] E.D. Macklen, Thermistors, Electrochemical Publications Limited, 1979.
[2] E. Jabry, G. Boissier, A. Rousset, R. Carnet, A. Lagrange, J Phys Colloq 46 C1 (1986) 843.
[3] J.P. Caffin, A. Rousset, R. Carnet, A. Lagrange, in: P. Vincenzini (Ed.), High-Tech Ceramics, Elsevier, Amsterdam, 1987, p. 1743.
[4] R. Legros, R. Metz, J.P. Caffin, A. Lagrange, A. Rousset, Mater Res Soc Symp Proc 121 (1988) 251.
[5] R. Metz, J.P. Caffin, R. Legros, A. Rousset, J Mater Sci 24 (1989) 83.
[6] M.L. Martínez Sarrión, M. Morales Sánchez, J Mater Chem 3 (3) (1993) 273.
[7] A. Feltz, J. Töpfer, F. Schirrmeister, J Eur Ceram Soc 9 (1992) 187.
[8] M.L. Martínez Sarrión, M. Morales Sánchez, J Am Ceram Soc 78 (4) (1995) 915.
[9] J. Töpfer, J. Jung, Thermochim Acta 202 (1992) 281.
[10] X.-X. Tang, A. Manthiram, J.B. Goodenough, J Less-Common Met 156 (1989) 357.
[11] C. Laberty, P. Alphonse, J.J. Demai, C. Sarda, A. Rousset, Mater Res Bull 32 (2) (1997) 249.
[12] J.L. Martin de Vidales, R.M. Rojas, E. Vila, O. Garcia Martinez, Mater Res Bull 29 (11) (1994) 1163.
[13] F.C.M. Driessens, G.D. Rieck, J Inorg Nucl Chem 28 (1966) 1593.
[14] J.V. Dubrawski, React Solids 2 (1987) 315.
[15] R. Metz, Thesis, Université Paul Sabatier, Toulouse (1991).
[16] D.G. Wickham, J Inorg Nucl Chem 26 (1964) 1359.
[17] E.H. Jabry, Thesis, Université Paul Sabatier Toulouse, 1985.
[18] S. Fritsch, Thesis, Université Paul Sabatier, Toulouse, 1995.
[19] O. Fruhwirth, A. Macher, K. Reichmann, H.G. Schuster, in: P. Duran, J.F. Fernandez (Eds.), Third Euro-Ceramics, Vol. 2. Properties of Ceramics, Faenza Editrice Iberica, Madrid (1993), p. 395.
[20] A. Miller, J Appl Phys (Suppl) 30 (1959) 245.
[21] J.B. Goodenough, A. Loeb, Phys Rev 98 (2) (1955) 391.
[22] H.St. C. O'Neill, A. Navrotsky, Am Mineral 68 (1983) 181.
[23] A. Feltz, A. Seidel, Z Anorg Allg Chem 608 (1992) 166.
[24] P. Poix, Bull Soc Chim 5 (1965) 1085.
[25] R. Legros, R. Metz, A. Rousset, J Mater Sci 25 (1990) 4410.
[26] B. Gillot, J.L. Baudour, F. Bouree, R. Metz, R. Legros, A. Rousset, Solid State Ionics 58 (1992) 155.
[27] M. Rosenberg, P. Nicolau, R. Manaila, P. Pausescu, J Phys Chem Solids 24 (1963) 1419.